Structure Comparison of Early and Late Lanthanide(III) Homodinuclear Macrocyclic Complexes with the Polyamine Polycarboxylic Ligand H_8OHEC

Ulrike A. Böttger,[a] Brendon O'Sullivan,[b] Burkhard Ziemer,[a] Herbert Schumann,[b] Clemens Mügge,[a] and Hardy Weißhoff*[a]

Keywords: Solid-state structures / Lanthanides / Macrocyclic ligands / Polyamine polycarboxylic acid / Solution thermodynamics

The solid-state structures of two new homodinuclear chelate complexes with the late lanthanide(III) ions Yb and Lu, $[Na_2(Yb_2OHEC)]\cdot 14.5H_2O$ (**1**), and $[Na_2(Lu_2OHEC)]\cdot 14.5H_2O$ (**2**) (H_8OHEC = 1,4,7,10,14,17,20,23-octaazacyclohexacosane- 1,4,7,10,14,17,20,23-octaacetic acid), have been determined by X-ray crystal structure analysis. Each lanthanide(III) ion is coordinated by eight donor atoms of the ligand and the geometry of the coordination polyhedron approaches a bicapped trigonal prism. These structures are compared with those of the homodinuclear chelate complexes with the same ligand and the mid to early lanthanide(III) ions Gd, Eu, La and also Y. A distinctive structural change occurs across the lanthanide series. The centrosymmetric mid to early lanthanide(III) complexes are all ninefold-coordinated in a capped square antiprismatic arrangement with a water molecule coordinated in a prismatic position. This structure is maintained in aqueous solution, together with an asymmetric minor isomer. The late lanthanide(III) OHEC complexes not only lack the inner-sphere water, but the change of coordination sphere also results in a loss of symmetry of the whole complex molecule. The observed change of coordination mode and number of the lanthanide ion may offer a geometric model for the isomerization process in eight- and ninefold-coordinated complex species that are isomers in a possible coordination equilibrium observed by NMR in aqueous solution. This model may also explain the intramolecular rearrangements necessary during water exchange in the inner coordination sphere of the complex $[(Gd_2OHEC)(H_2O)_2]^{2-}$ through a slow dissociative mechanism. Protonation constants of the H_8OHEC ligand and complex formation constants of this ligand with Gd^{III}, Ca^{II}, Cu^{II} and Zn^{II} have been determined by solution thermodynamic studies.

Introduction

H_8OHEC (1,4,7,10,14,17,20,23-octaazacyclohexacosane-1,4,7,10,14,17,20,23-octaacetic acid) is a macrocyclic polyaminocarboxylate with a 26-atom-membered ring formed from the eight amine and bridging ethylene or propylene groups. It was developed as a potential MRI contrast agent ligand, combining two aims: (i) to increase the rotational correlation time compared with conventional DOTA and DTPA, thereby enhancing the relaxivity, the measure of drug efficiency; (ii) to obtain previously unknown binuclear contrast agents with two closely sited gadolinium ions, and to study the intramolecular interaction of the two paramagnetic centres as well as their influence on the electronic relaxation. Previous studies focussed on the preparation[1] of this ligand and its properties as a chelator for lanthanides and small transition metals.[2] The crystal structures of the homodinuclear complexes of yttrium(III), gadolinium(III), europium(III), and lanthanum(III) with H_8OHEC have been discussed, as well as the solution structure and dynamics of its diamagnetic Y^{III} complex.[2,3] These complexes are almost isostructural in that they all crystallise in the monoclinic space group $P2_1/n$, and the conformation of the OHEC macrocycle as well as the coordination geometry around the metal ions is nearly the same. NMR studies on the yttrium complex revealed that the same centrosymmetric structure is maintained in aqueous solution as is found in the solid state. In addition, in aqueous solution the complexes are present in two isomeric forms.[3,4] The doubled NMR signal number of the second isomer obviously reveals an asymmetrical molecule, the geometry of which could not be deduced from the NMR spectroscopic data because of strongly overlapping signals with those of the main isomer.

Coordination polyhedra of the ninefold-coordinated complexes investigated by X-ray crystal structure analysis were interpreted with special regard to their metal-bound water molecule in the inner coordination sphere. A second inspection showed that these structures must be reconsidered. In this report they will be discussed anew together with the structures of two new homodinuclear OHEC com-

[a] Institut für Chemie, Humboldt Universität zu Berlin, Brook-Taylor-Str. 2, 12489 Berlin, Germany
Fax: (internat.) + 49-(0)30-2093-7561
E-mail: weiss@chemie.hu-berlin.de
[b] Institut für Chemie, Technische Universität Berlin, Strasse des 17. Juni 135, 10623 Berlin, Germany

  DOI: 10.1002/ejic.200400124

plexes with the late lanthanides ytterbium(III) and lutetium(III).

The acidity constants of H_8OHEC and the thermodynamic stabilities of its complexes formed with Gd^{3+}, Ca^{2+}, Cu^{2+} and Zn^{2+} are reported here. These metals were chosen to examine the in vivo stability and selectivity of OHEC complexed gadolinium with respect to its possible application as a contrast agent for magnetic resonance imaging.

Results and Discussion

X-Ray Crystal Structures

Molecular Structures of 1 and 2

The crystals contain $[C_{34}H_{52}Ln_2N_8O_{16}]^{2-}$ anions, sodium cations, hydroxide ions, ethanol molecules and water of crystallization. Their compositions correspond to $[Na_2(Yb_2OHEC)]\cdot 14.5H_2O$, C_2H_5OH, 0.5NaOH (**1**) and $[Na_2(Lu_2OHEC)]\cdot 14.5\cdot H_2O$, C_2H_5OH, 0.5NaOH (**2**). The complexes are isostructural and crystallise in the triclinic space group $P\bar{1}$ (no. 2), which is centrosymmetric. There are the two molecules of the complex per unit cell, which are connected via sodium cations and are centrosymmetric with respect to each other. Crystals are built up from infinite one-dimensional chains of $[Ln_2(OHEC)]^{2-}$ units, arranged parallel to the *a* axis and linked by a network of $Na^+\cdots O$ contacts, involving the sodium cation, the carboxylate oxygen atoms and the water molecules associated with the cation. Thus, although **1** and **2** lack the inner-sphere water molecules, the complexes are wrapped in a water matrix. The shortest distances between bulk water molecules and metal ion centres are 430(14) ($O_{aqua(18)}-Yb_1$) / 453(8) pm ($O_{aqua(32)}-Yb_2$) for **1** and 432(5) ($O_{aqua(18)}-Lu_1$) / 451(10) pm ($O_{aqua(32)}-Lu_2$) for **2**. As the centre of symmetry lies outside the complex molecule, the two chemically identical halves of the complex molecules **1** and **2**, containing the Yb^{III} and Lu^{III} ions, respectively, can only be interconverted by a pseudo-C_2 symmetry operation. The complex molecule itself possesses no kind of symmetry.

Conformation of the Macrocycle in Lanthanide OHEC Complexes

The two lanthanide ions in **1** and **2** are completely encapsulated by the macrocyclic ligand (Figure 1). Each lanthanide ion is coordinated by the four nitrogen and four carboxylic oxygen atoms belonging to one-half of the overall hexadecadentate ligand.

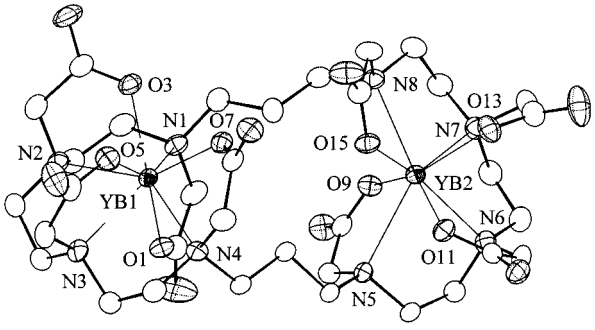

Figure 1. Solid-state conformation of $Na_2(Yb_2OHEC)$ (**1**)

Figure 2 shows the overall conformation of the OHEC macrocycle in the di-ytterbium complex **1**, together with the qualitative torsion angles. Measured torsion angles are listed in Table 1. In contrast to the light lanthanide(III) OHEC complexes, the rings of which adopt a centrosymmetric biangular conformation, {1313}, according to the terminology of Dale[5], the complexes with the smaller and heavier lanthanides ytterbium(III) and lutetium(III) form quadrangular ring conformations with four genuine corners, {7272}. This leads to essentially tighter folding of the ring around the central atoms, leaving no room for an inner-sphere water molecule. The fivefold repetition of *anti* torsion angles in the propylene chains allows for a maximal

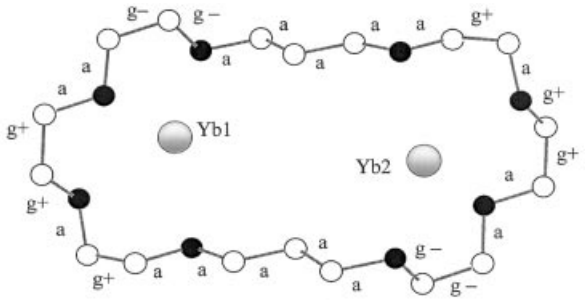

Figure 2. Conformation of the OHEC ligand in **1**, with corresponding qualitative torsion angles

Table 1. Measured torsion angles (°) of the OHEC macrocycle in the di-ytterbium complex **1**

Torsion angle				**1**	**2**
N1	C1	C2	N2	64.87(37)	65.76(46)
C1	C2	N2	C3	−170.81(27)	−171.33(34)
C2	N2	C3	C4	97.49(31)	96.84(39)
N2	C3	C4	N3	52.35(36)	52.43(45)
C3	C4	N3	C5	−171.13(26)	−171.17(34)
C4	N3	C5	C6	170.04(26)	169.43(34)
N3	C5	C6	N4	−63.45(34)	−63.41(44)
C5	C6	N4	C7	−88.08(31)	−89.09(39)
C6	N4	C7	C8	174.64(26)	174.44(33)
N4	C7	C8	C9	172.93(26)	173.01(32)
C7	C8	C9	N5	156.15(25)	157.11(329
C8	C9	N5	C10	170.64(25)	170.16(32)
C9	N5	C10	C11	−168.83(25)	−169.60(33)
N5	C10	C11	N6	66.07(33)	67.63(44)
C10	C11	N6	C12	170.86(26)	−168.59(34)
C11	N6	C12	C13	95.52(31)	93.3(4)
N6	C12	C13	N7	57.46(35)	57.85(45)
C12	C13	N7	C14	−171.74(27)	−173.27(34)
C13	N7	C14	C15	165.02(28)	167.14(34)
N7	C14	C15	N8	−65.33(36)	−67.30(43)
C14	C15	N8	C16	−87.45(33)	−85.48(40)
C15	N8	C16	C17	177.41(27)	175.73(35)
N8	C16	C17	C18	174.67(26)	174.50(34)
C16	C17	C18	N1	154.72(27)	155.49(35)
C17	C18	N1	C1	169.72(27)	170.87(34)
C18	N1	C1	C2	−167.96(27)	−168.67(35)

separation of the two lanthanides, thereby minimizing electrostatic repulsion.

While the centrosymmetric conformation of the macrocyclic ring of the lighter lanthanide(III) OHEC complexes[3] as well as for the corresponding OHEC-amine ligand and its binuclear copper(II) complex $[Cu_2(OHEC\text{-}amine)](SO_4)_2$ [1] corresponds to the chair shape, for **1** and **2** the ring adopts the boat conformation with a typical pseudo-C_2 symmetry axis. In the OHEC complexes with the chair shape the central atoms as well as the inner-sphere water molecules lie alternately below and above a mean ring plane of the macrocycle, formed by the four propylene bridged nitrogen atoms.[1,3] No such mean plane is found for **1** and **2**. Here, the metal ions both sit on the same side, within the boat conformation of the macrocyclic ring. They are, in each case, sandwiched between nitrogen atoms and three carboxylate arms coordinating the metal from the upper side of the boat, while the forth carboxylate side arms fixed on N1 and N5 coordinate the metals from the lower side of the boat. The layout of the acetate arms depends on the inherent symmetries of these two types of rings. Whereas in the centrosymmetric conformations the pendent arms with up-up-up-down orientations are inverted for both molecule halves at the centre of symmetry, in the boat conformation the up-up-up-down orientations of the four pendant arms of each molecule half can be only interconverted by rotation around a pseudo-C_2 symmetry axis.

Coordination Geometry of the Late Lanthanide Ions

The two lanthanide ions in **1** and **2** are chelated by the hexadecadentate ligand H_8OHEC and adopt eight-coordinate geometry. The coordination sphere for each lanthanide ion consists of four amine nitrogens of the macrocycle and four carboxylic oxygens of the acetate side arms. The large OHEC-ring system is quite flexible but the accommodation of two lanthanide ions is a considerable steric demand. As all eight nitrogen donor atoms belong to one large macrocyclic system they experience a steric constraint. Moreover, as all faces of the polyhedra are built up by mixed donor atoms, by nitrogen atoms and carboxylate oxygens, significant deviations from the ideal geometry can be expected.

Using the criterion established by Haigh for distinguishing the types of structures in eightfold-coordinated complexes, based on a pattern of bond angles,[6] the 28 LML′ angles at the central atom the 16th, 17th and 18th lowest angles were compared. For Yb1 in **1** these are 91.99°, 97.22° and 118.60°, for Lu1 in **2** the corresponding values are 92.93°, 95.71° and 117.42°. The structure should be square antiprism (SAP) if the gap between the 16th and 17th lowest angles is more than 20°. This is not the case. As the gap between the 17th and 18th lowest LML′ angles is substantial the structure should be close to a bicapped trigonal prism (BCTP) (Figure 3). Compared with reclassified structures,[6] on the basis of Haigh's criterion the gap in **1** and **2** is large enough to assign the structure as distorted BCTP. The third possibility, a triangular dodecahedron, must be ruled out as the 16th, 17th and 18th LML′ angles are not close together.

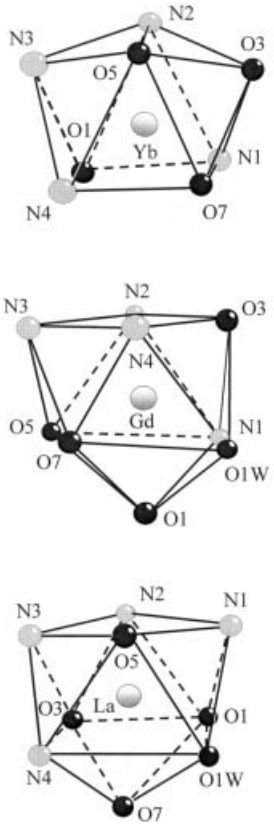

Figure 3. Coordination polyhedron about the ytterbium ion in **1** (top), gadolinium ion in **4** (middle) and lanthanum ion in **6** (bottom)

Comparison of the dihedral angles δ in the primary coordination sphere of the central atoms of **1** and **2**, which are sensitive to symmetry and shape, with those of an ideal D_{4d} (SAP) and C_{2v} (BCTP) geometry gives a more objective assessment of shape (Table 2).[7] The observed deviations from the ideal indicate the ligand's difficulty in satisfying the steric demands of the two central atoms. Of the two alternative polyhedra the polytopal shape of **1** and **2** is best described with the distorted BCTP geometry. For a SAP geometry the two square planes that should be nearly parallel to each other could not be found. Deviations from planarity of the second face are too large (Table 2).

The three different lengths of the prismatic heights of the coordination cage is also a measure of distortion from the ideal BCTP (Table 2). Therefore, the triangular faces of the polyhedra are far from being parallel.

For Yb1 in **1**, atoms N4, O7, O5 and O1, N1, N2 form the triangular faces and the capping positions are occupied by N3 and O3 (Figure 3). For Yb2 in **1** and the two Lu atoms in the isostructural complex **2** the same coordination geometry is found. The metal ions are close to the centre of the trigonal prism, slightly shifted toward the face capped with an acetate oxygen atom and shifted down toward the triangular face of the trigonal prism containing two oxygen donor atoms. The mean $Lu-O_{carboxylate}$ bond

Table 2. Dihedral angles δ in eightfold coordination for lanthanide OHEC complexes. Estimated standard deviation of last reported digit in parentheses

Complex	δ in coordination cages	Angle (°)	Idealized angle (°)
1 (Yb1)	O1−N1−O7−N4	−0.09(10)	0.0 (BCTP); 0.0 (SAP)
	N3−O5−O3−N2	23.41(11)	21.8 (BCTP); 0.0 (SAP)
	N3−O1−N2−N1	28.18(15)	48.2 (BCTP); 52.4 (SAP)
	O1−N2−N1− O3	63.48(12)	48.2 (BCTP); 52.4 (SAP)
	N3−N4−O5−O7	44.36(12)	48.2 (BCTP); 52.4 (SAP)
	O3−O7−O5−N4	45.20 (11)	48.2 (BCTP); 52.4 (SAP)
1 (Yb2)	O15−N8−O9−N5	−0.07(13)	0.0 (BCTP); 0.0 (SAP)
	N7−N6−O11−O13	−26.62(11)	21.8 (BCTP); 0.0 (SAP)
	N7−O9−N6−N5	25.59(13)	48.2 (BCTP); 52.4 (SAP)
	O11−N5−N6− O9	64.46(11)	48.2 (BCTP); 52.4 (SAP)
	N7−O13−N8− O15	40.85(13)	48.2 (BCTP); 52.4 (SAP)
	O11−O15−O13−N8	44.21(12)	48.2 (BCTP); 52.4 (SAP)
1 (Yb1)	N3−O5−N2−O3	−151.39(14)	0 (SAP)
	N4−O1−O7−N1	−179.89(13)	0 (SAP)
1 (Yb2)	N5−O15−O9−N8	179.93(13)	0 (SAP)
	O11−N6−O13−N7	−145.42(14)	0 (SAP)
2 (Lu1)	O1−N1−O7−N4	−0.18(12)	0.0 (BCTP); 0.0 (SAP)
	N2−O3−O5−N3	22.68(13)	21.8 (BCTP); 0.0 (SAP)
	N3−O1−N2−N1	28.54(15)	48.2 (BCTP); 52.4 (SAP)
	O1−N2−N1− O3	63.52(13)	48.2 (BCTP); 52.4 (SAP)
	N3−N4−O5−O7	45.08(15)	48.2 (BCTP); 52.4 (SAP)
	O3−O7−O5−N4	43.54(14)	48.2 (BCTP); 52.4 (SAP)
2 (Lu2)	O15−N8− O9−N5	0.19(13)	0.0 (BCTP); 0.0 (SAP)
	N7−N6−O11−O13	−27.52(12)	21.8 (BCTP); 0.0 (SAP)
	N7−O9−N6−N5	25.01(16)	48.2 (BCTP); 52.4 (SAP)
	O11−N5−N6−O9	65.4(14)	48.2 (BCTP); 52.4 (SAP)
	N7−O13−N8−O15	43.03(16)	48.2 (BCTP); 52.4 (SAP)
	O11−O15−O13−N8	43.32(14)	48.2 (BCTP); 52.4 (SAP)
2 (Lu1)	N3−O5−N2−O3	−152.39(16)	0 (SAP)
	N4−O1−O7−N1	−179.77(15)	0 (SAP)
2 (Lu2)	N5−O15−O9−N8	179.76(16)	0 (SAP)
	O11−N6−O13−N7	−143.99(16)	0 (SAP)
Edge lengths of the prismatic heights in the BCTP polyhedron [pm]			
	N4−O1	O5−N2	O7−N1
1	299(17)	341(14)	367(13)
2	296(19)	341(16)	361(19)
	O15−N5	O13−N6	N8−O9
1	367(17)	322(18)	293(18)
2	366(18)	324(17)	295(19)

length in **2** is 224.3 pm, slightly shorter than in the ninefold-coordinated Na[LuDOTA(H_2O)] complex (227.9 pm).[8] Also, the mean Lu−N distance in **2** (254.9 pm) is shorter than in Na[LuDOTA(H_2O)] (261.4 pm). Consistent with the lanthanide contraction the mean distances in **1** are slightly longer than in **2** (mean Yb−$O_{carboxylate}$ 225.4 pm and mean Yb−N 256.3 pm). For the eight-coordinate K[Tm(DOTA)],[9] a complex with the lanthanide ion next to Yb^{3+} in the periodic table, the mean Tm−$O_{carboxylate}$ distance of 228 pm is, as expected, longer than in **1**, whereas the mean Tm−N distance of 252.9 pm is slightly shorter than in **1** and also than in **2**.

Table 3 lists the Ln−O and Ln−N distances of LnOHEC complexes, which reflect well the shrinkage of the ionic radii of the chelated lanthanide ions.

The differences between the maximum and minimum interatomic distances in **1** and **2** (Table 4) are too small to indicate distortions within the molecule caused by steric constraints.

Coordination Geometry of the Early to Mid Lanthanide Ions: Implications for the Inner-sphere Water Exchange and an Isomeric Coordination Equilibrium

Since Ln^{3+} aqua ions and other polyaminocarboxylate complexes have varying hydration numbers throughout the series, a varying coordination number may be expected in OHEC lanthanide complexes, depending upon the size of the Ln^{3+} cation.[10]

In the early to mid di-lanthanide complexes of the H_8OHEC ligand the central atoms are all ninefold-coordi-

Table 3. Bond lengths in the metal coordination sphere

	(1)Yb	(2) Lu	(3)Y	(4)Gd	(5)Eu	(6)La
Ln(1)−O(1)	222.7(2)	221.8(3)	241.2(2)	246.5(3)	247.7(4)	252.9(5)
Ln(1)−O(3)	230.0(2)	229.1(3)	228.4(3)	234.9(3)	236.2(4)	246.4(5)
Ln(1)−O(5)	226.0(2)	224.9(3)	233.7(3)	235.9(3)	237.2(4)	246.4(5)
Ln(1)−O(7)	222.8(2)	221.4(3)	230.7(3)	234.7(3)	236.5(5)	252.9(5)
Average	225.4	224.3	233.5	238.0	239.4	249.6
Ln(1)−O(1W)	−	−	236.3(3)	240.6(3)	243.0(5)	252.6(6)
Ln(1)−N(1)	265.3(3)	264.8(3)	264.7(3)	262.3(4)	265.4(5)	275.3(6)
Ln(1)−N(2)	249.9(3)	248.0(3)	266.2(3)	269.3(3)	271.1(5)	277.6(6)
Ln(1)−N(3)	252.1(3)	250.1(4)	265.2(3)	270.0(3)	270.6(5)	277.6(6)
Ln(1)−N(4)	258.0(3)	256.9(3)	276.7(3)	276.7(4)	279.9(5)	275.4(6)
Average	256.3	254.9	268.2	269.6	271.8	276.5
Ln(1)−Ln(2)	658(8)	662(19)	665(3)	652(1)	652(2)	636(2)

nated.[2,3] Besides the eight donor atoms per metal ion provided by the ligand the ninth site in the metal coordination sphere is occupied by a water molecule. In most such polyamine polycarboxylate ligand complexes the oxygen atom of the inner-sphere water molecules occupies a special site in the coordination polyhedron: it takes a capping position both in the square antiprismatic structures in DOTA-like complexes[11,12] and in the trigonal prismatic structures of acyclic ligand complexes, e.g. as in $[Gd(BOPTA)(H_2O)]^{2-}$.[13]

Initial discussion regarding the structure of homodinuclear OHEC complexes $[Na_2(Y_2OHEC)(H_2O)_2]$ (**3**), $[Na_2(Gd_2OHEC)(H_2O)_2]$ (**4**), $[Na_2(Eu_2OHEC)(H_2O)_2]$ (**5**) and $[Cs_2(La_2OHEC)(H_2O)_2]$ (**6**) was led by the thought that the water molecule should occupy a capping position, as in the DOTA complexes, resulting in an irregular coordination polyhedron. After reinspecting the lanthanide environment in these complexes we found, in all cases, a distorted capped

Table 4. Selected structural parameters for lanthanide OHEC complexes

Complex (Ln)	C−N [pm]	C−C [pm]	$C-O_{carboxylate}$ [pm]	$C-O_{keto}$ [pm]
1 (Yb)	148.1−149.9(4)	150.0−153.6(4)	126.5−128.9(4)	123.1−124.9(5)
2 (Lu)	147.7−149.5(5)	150.0−153.4(5)	126.5−128.4(5)	121.7−124.4(5)
3 (Y)	147.9−150.8(5)	150.5−152.8(5)	124.9−128.4(5)	122.4−125.7(5)
4 (Gd)	146.8−149.9(5)	150.5−152.5(6)	125.8−128.9(5)	122.3−125.2(5)
5 (Eu)	146.9−150.1(9)	149.4−153.1(9)	123.1−125.4(8)	126.0−127.8(8)
6 (La)	146.3− 50.8(10)	150.0−154.4(10)	125.6−127.9(10)	122.2−125.0(9)

Table 5. Some face angles of the ninefold coordination polyhedra (OHEC complexes **3**−**6**)

Complex	Face 1	Face 2	Angle (°)	Idealized angle (polyhedron)
3	N1−N2−O5	N4−O7−O1W	27.4	0 (TTP)
	N3−N2−N4	O3−N2−N4	0.73	0 (CSAP)
	O5−O7−N1	O1−W−O7−N1	1.21	0 (CSAP)
	N2−N3−N4−O3	N1−O5−O7−O1W	4.5	0 (CSAP)
4	N1−N2−O5	N4−O7−O1W	27.6	0 (TTP)
	N3−N2−N4	O3−N2−N4	−0.83	0 (CSAP)
	O5−O7−N1	O1−W−O7−N1	1.03	0 (CSAP)
	N2−N3−N4−O3	N1−O5−O7−O1W	5.5	0 (CSAP)
	N7−O13−O15	N5−O11−O3W	17.8	0 (TTP)
	N6−N7−O11	N8−N7−O11	−178.74	0 (CSAP)
	N5−O13−O3W	O15−O13−O3W	−177.94	0 (CSAP)
	N6−N7−N8−O11	N5−O13−O15−O3W	6.2	0 (CSAP)
5	N1−N2−O5	N4−O7−O1W	27.8	0 (TTP)
	N3−N2−N4	O3−N2−N4	0.2	0 (CSAP)
	O5−O7−N1	O1−W−O7−N1	−1.18	0 (CSAP)
	N2−N3−N4−O3	N1−O5−O7−O1W	5.7	
	N7−O13−O15	N5−O11−O2W	16.9	
	N6−N7−O11	N8−N7−O11	−179.57	
	N5−O13−O2W	O15−O13−O2W	−177.63	
	N6−N7−N8−O11	N5−O13−O15−O2W	6.5	
6	N2−N3−N4−O3	N1−O5−O7−O1W	5.7	0 (CSAP)
	N2−O1−O3	N4−O5−O1W	13.7	0 (TTP)
	N3−N2−O5	N1−N2−O5	−5.5	0 (CSAP)
	O3−N4−O1	O1−W−O1−N4	2.38	0 (CSAP)
	N1−N2−N3−O5	N4−O1−O3−O1W	8.5	0 (CSAP)

square antiprism (CSAP) as coordination polyhedron, as in DOTA-like complexes but, importantly, the inner-sphere water molecule occupies a prismatic position instead of a capping one (Figure 3). The positions of both square faces are occupied by mixed donor atoms of the ligand. For **3**, **4** and **5** the uncapped square is formed by three ring nitrogens (N2, N3 and N4) and O3, whereas the capped square face is formed by N1, two carboxylate oxygens, O5 and O7, and one inner-sphere water oxygen O1W. Considering the coordination geometry in **6** as a strongly distorted CSAP structure, the uncapped square is formed by N1, N2, N3 and O5. The capped square face is formed by N4, two carboxylate oxygens, O1 and O3, and one inner-sphere water oxygen O1W. For the gadolinium(III) complex **4** the polyhedron comes closest to the ideal CSAP structure. The uncapped square face deviates from planarity by less than 1°. Lanthanum(III) structure **6** shows the highest deviation (Figure 3). Table 5 summarises the most important angles characterising the coordination cage of the lanthanide ions in the four OHEC complexes.

The change of coordination number from nine for the early to mid lanthanides to eight for the late lanthanides in the same type of chelate complex as a result of the lanthanide contraction has been well investigated by NMR for lanthanide(III) DOTA complexes,[9,14] and has also been observed for other polyamine polycarboxylate ligands.[15,16] For lanthanide OHEC complexes, the change of complex geometry is accompanied by a loss of symmetry. This is clearly observable upon considering the CO−CH_2 connectivities in the HMBC spectra of the centrosymmetric Y_2OHEC (**3**, four cross peak pairs) and Lu_2OHEC without a centre of symmetry (**2**, eight cross peak pairs) (Figure 4).

For DOTA complexes, besides the two enantiomeric pairs of ninefold-coordinated stereoisomers, differing in the ligand conformation, a coordination change is superimposed.[14] The loss of the metal-bound water molecule leads to two further structures in which the metal ion is only eight-coordinate but where the coordination geometries are fundamentally maintained since the departing inner-sphere water occupies the capping position in a squared antiprism. This peculiar capping site provides a readily accessible intermediate to water exchange via a more dissociatively activated mechanism for the gadolinium(III) complexes,[17] which yields relatively rapid exchange rates, with $k_{ex}(298)$ in the range of 4.1×10^6 s^{-1} for DOTA[18] and 1.6×10^6 s^{-1} for DO3A−bz−NO_2 [19] for such compounds. As the square antiprism for DOTA-like complexes is unchanged during the exchange process for all investigated lanthanide(III) complexes, there is little difference in the energies between the nine- versus eight-coordinate complexes. Thus, despite the high rigidity of the inner-sphere structure in DOTA complexes the activation energy for the water exchange reaction is very small.[14]

NMR investigations of the di-yttrium complex **3** show that its geometry in aqueous solution is very similar to that in the solid state.[3,11] For each complex, two isomers undergoing conformational changes were proven. Interchange from the major to the minor isomer is accompanied by a loss of centrosymmetry. Figure 5 shows this by means of the Eu_2OHEC ^{1}H NMR spectrum. The same observations have been made for the lanthanide OHEC complexes with Ln^{III} = Eu, Gd, and Tb by means of NMR, UV/Vis, EPR and luminescence spectroscopy.[4] For the europium complex **5** and the gadolinium complex **4** the metal centres change their coordination number from 9 to 8 during isomerisation equilibrium, such as $[Ln_2(OHEC)_2(H_2O)_2]^{2-} \rightarrow [Ln_2(OHEC)]^{2-} + 2H_2O$. As the structures of these two isomers correspond to the two structure types of lanthanide OHEC complexes found in the solid state, the major isomer must have a centrosymmetric, nine-coordinate CSAP structure while the minor isomer has the distorted eight-coordinate BCTP structure without molecular symmetry. Therefore, the isomeric equilibrium not only involves changes of conformation but also of coordination. Figure 6 depicts the rearrangement of the complex molecule in an exchange equilibrium between the two isomers. In contrast to DOTA-like complexes, a water molecule that enters or leaves the metal coordination sphere in lanthanide OHEC complexes gives rise to a considerable reorganisation of the donor atoms and the ring conformation about the metal atom, as the inner-sphere water is less accessible at a prismatic position of the coordination polyhedron. Notably, this rearrangement does not require the release of ligand donor coordination bonds, while removal of the metal-bound water molecules, which are also stabilised by hydrogen bonds, can be considered as the first step in the isomerisation process.

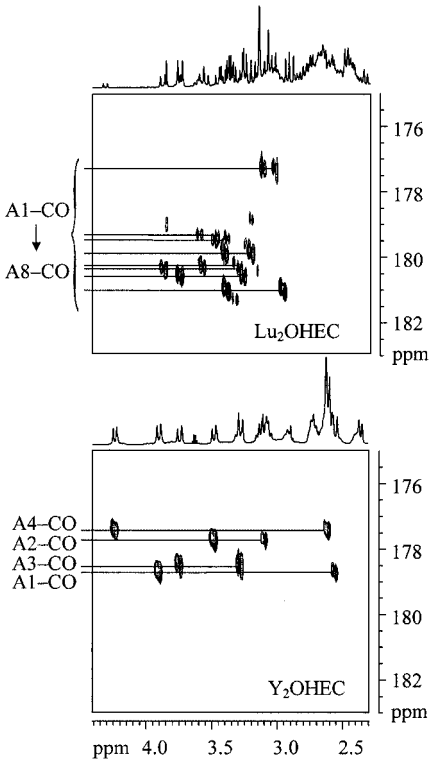

Figure 4. CO−CH_2 region of the HMBC spectra of Lu_2OHEC (**2**, top) and Y_2OHEC (**3**, bottom); there are twice as many NMR cross peaks for Lu_2OHEC than for the main isomer of Y_2OHEC, which can be correlated directly with the loss of symmetry

During the structural change, only four of the eight donor atoms nearly keep their positions. The N1 atom, which carries the O1 atom, is probably moved by a conformational change of the macrocycle. Simple rotation of the acetate arms can accomplish all other changes of positions.

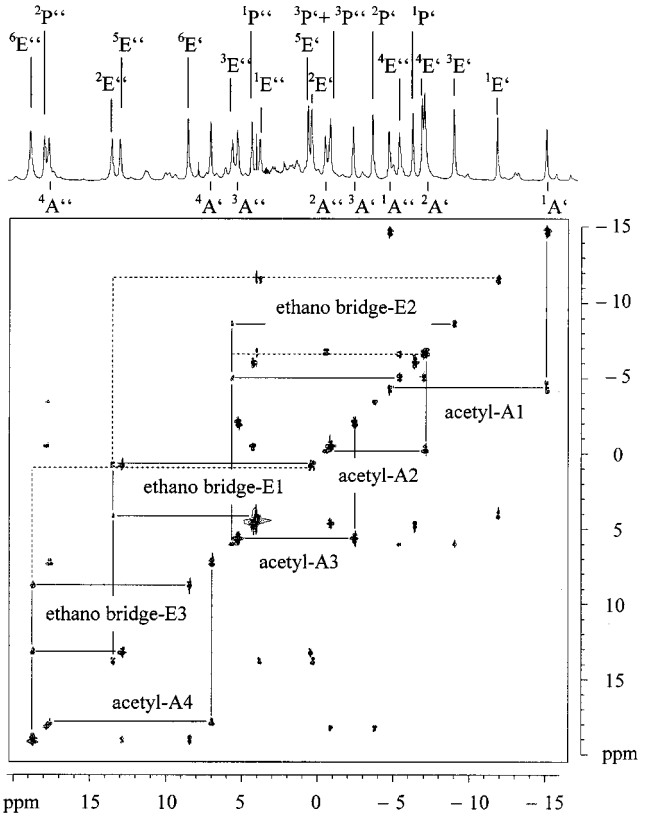

Figure 5. $^1H-^1H$ COSY spectrum of the binuclear Eu^{III} complex of OHEC at 600 MHz; assignment of the centrosymmetric, major isomer $Eu_2OHEC(H_2O)_2$ is shown; the protons can be classified into three ethylene groups (ethano bridge E1−E3, consisting of protons $^1E/^2E$, $^3E/^4E$ and $^5E/^6E$), four acetate arms A1−A4 and one propylene group; the symbols ′ and ″ refer to two geminal protons; assignment of the protons of the minor isomer, preformed using exchange spectroscopy (EXSY), is not shown for clarity

These ligand rearrangements, which take place simultaneously in both halves of the molecule, may account for the extremely slow isomerisation rate [$k_{is}(298) = 73.0\ s^{-1}$] and the very slow water exchange rate [$k_{ex}(298) = 0.40 \times 10^6\ s^{-1}$] in the $[Gd_2OHEC(H_2O)_2]^{2-}$ complex.[4] The rate constant is similar to that of DTPA-bis(amides).[18,20]

Interaction of this inner-sphere water with the gadolinium(III) ion and its exchange with bulk water is the basis for the action of MRI contrast agents of such compounds. However, the distances between the gadolinium atom and the water oxygen atom, and between the gadolinium atom and the acetate oxygen atom in most known polyamine polycarboxylate structures, show that the water ligand does not bind at an exceptionally different distance. Thus, the preferred capping position in DOTA-like complexes for the water molecule, as discussed above, results not from constraints imposed by the donor atoms but rather results from the favourable preorganisation of the ligand. The exchange process is fast on the proton NMR time scale, so that two isomers differing only in the water coordination number while retaining the same ligand conformation are indistinguishable.

Solution Thermodynamics

Potentiometry

Potentiometric titration data for the ligand OHEC may be represented conveniently by calculation of the average number of ligand-bound protons ($\tilde{n}_H$) for each point in the titrations, as in Figure 7. Equation (1) defines $\tilde{n}_H$ in terms of K_w, the ionisation constant of water, H_T and L_T, the total (analytical) concentrations of protons and the ligand, respectively, and $[H^+]$ the concentration of free protons. Notably, $\tilde{n}_H$ is calculated entirely from observable param-

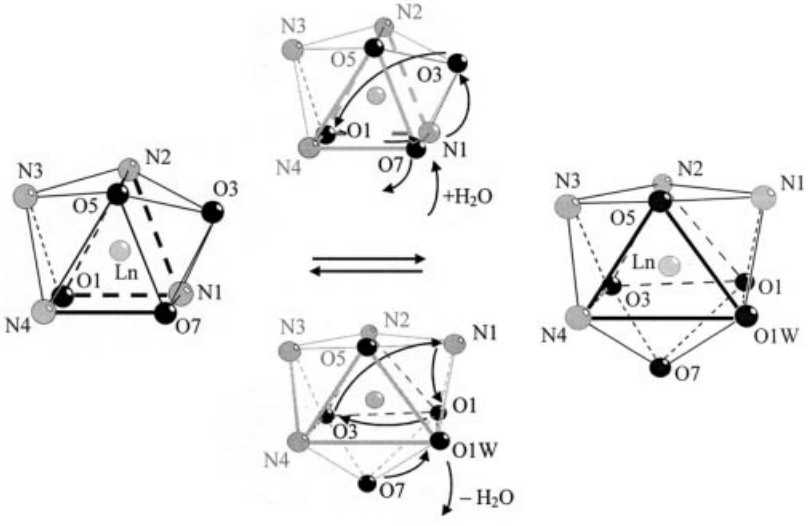

Figure 6. Coordination equilibrium for isomers of lanthanide(III) OHEC complexes

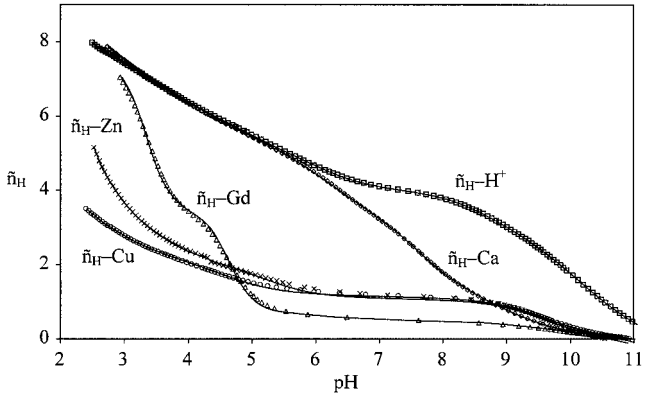

Figure 7. Average number of protons bound ($\tilde{n}_H$) to the ligand OHEC in the presence of the indicated metals, where H^+ indicates the absence of any coordinating metal ion; symbols give observed titration curves and lines the calculated fits to those curves; data were obtained using metal-to-ligand ratios for Cu of 1.9:1, Zn 1.95:1, Ca 1.86:1 and Gd 1.75:1

eters (observed pH and the analytical concentrations) and is, therefore, independent of the chemical model used to extract stability constants from the data. Thus, careful inspection of $\tilde{n}_H$ curves will reveal insights into the chemical equilibria present, and act as a guide in model selection. The solid lines in Figure 7 also give the $\tilde{n}_H$s as derived from the calculated pH. In this manner, the quality of fit between the observations and the refinements is presented.

$$\tilde{n}_H = \frac{H_T - [H^+] + K_W \cdot [H^+]^{-1}}{L_T} \quad (1)$$

All $\tilde{n}_H$ curves in Figure 7 approach zero above pH 11. In this highly basic region, OHEC forms only fully deprotonated species, either as the free ligand or as the various metal complexes. At lower, more acidic pHs, the $\tilde{n}_H-H^+$ curve climbs rapidly, indicating protonation of the ligand with up to eight protons by pH 2.5. In fact the $\tilde{n}_H-H^+$ curve shows no sign of reaching a plateau at this level and more than eight protonation constants might be calculated (OHEC contains up to 16 acid/base donor groups). This was indeed possible, giving protonation constants up to β_{019} (Table 6). The remaining protonation constants up to the 16th value are too acidic to allow measurement by conventional potentiometry.

The $\tilde{n}_H$ curve for Ca^{2+} coincides with that of $\tilde{n}_H-H^+$ below pH 6. Thus, for the conditions of the titration, no coordination with calcium is expected below pH 6, with relatively weak complexation at higher pHs. Indeed, the constants for calcium are the smallest of all metals in Table 6 and the distribution diagram of Figure 8 confirms the absence of calcium-binding below pH 6.

In contrast, OHEC is bound very strongly by Cu^{2+} and Zn^{2+}, affording $\tilde{n}_H$ curves well displaced from that for $\tilde{n}_H-H^+$, even at the strongly acidic pH of 2.5. In fact, the 3.5 protons that remain bound to OHEC at pH 2.5 in the presence of Cu^{2+} are barely enough to allow measurement of the stability constants by potentiometry. Interestingly, both Cu^{2+} and Zn^{2+} generate $\tilde{n}_H$ curves with wide plateaus between pH 6 and 9 at one bound proton, revealing a highly stable M_2LH species, while complete deprotonation of the two metal-centre complex is observed only above pH 9. These observations are reflected in the complexation constants of Table 6 and the lowermost species distribution diagram of Figure 8, which is calculated from those constants.

Finally, Gd^{3+} displays a coordination strength with OHEC that is between those of Ca^{2+} and Cu^{2+}. Below pH 3 the curve $\tilde{n}_H-Gd^{3+}$ rapidly approaches that for $\tilde{n}_H$-H^+, indicating acidic liberation of Gd^{3+} from the ligand. At higher pH, coordination proceeds rapidly and is complete by pH 5.5. The species distribution diagram of Figure 8 with the end species reflects this behaviour, Gd_2L dominating from pH 6 and higher.

Table 6. Protonation and metal complexation constants determined for the ligand OHEC, defined as in Equation (2); figures in parentheses give the standard deviation (σ) expressed in units of the least significant figure of each constant, calculated from the variation between repeat determinations; *n* is the number of determinations for each constant. Note that for the protonation constants the index m is always zero. Logarithms calculated with the decimal basis ($\log_{10}$)

Species	m	l	h	*H* (*m* = 0) log β_{0lh}	n	Gd log β_{mlh}	n	Ca log β_{mlh}	n	Cu log β_{mlh}	n	Zn log β_{mlh}	n
ML	1	1	0			18.32 (2)	6	7.7 (3)	6	18.7 (4)	4	17.4 (3)	4
MLH	1	1	1	10.7 (1)	8	28.53 (9)	5	17.9 (3)	8	28.9 (3)	6	27.7 (1)	6
MLH_2	1	1	2	20.88 (2)	8	37.84 (8)	7	27.4 (3)	12	38.5 (3)	6	37.0 (1)	6
MLH_3	1	1	3	30.36 (4)	8	43.82 (8)	9	35.0 (2)	13	45.6 (2)	6	44.5 (2)	6
MLH_4	1	1	4	38.94 (1)	8	47.8 (1)	10			50.3 (4)	6	49.6 (3)	5
MLH_5	1	1	5	45.14 (4)	8							53.1 (3)	5
MLH_6	1	1	6	50.22 (6)	8								
MLH_7	1	1	7	54.15 (7)	8								
MLH_8	1	1	8	57.21 (4)	8								
MLH_9	1	1	9	59.5 (3)	8								
M_2L	2	1	0			33.6 (1)	8	13.8 (4)	8	36.4 (4)	4	33.4 (3)	6
M_2LH	2	1	1					22.8 (3)	7	45.9 (1)	5	42.9 (2)	6
M_2LH_2	2	1	2							50.5 (2)	6	48.0 (2)	6
M_2LH_3	2	1	3							53.8 (3)	6	51.5 (2)	5

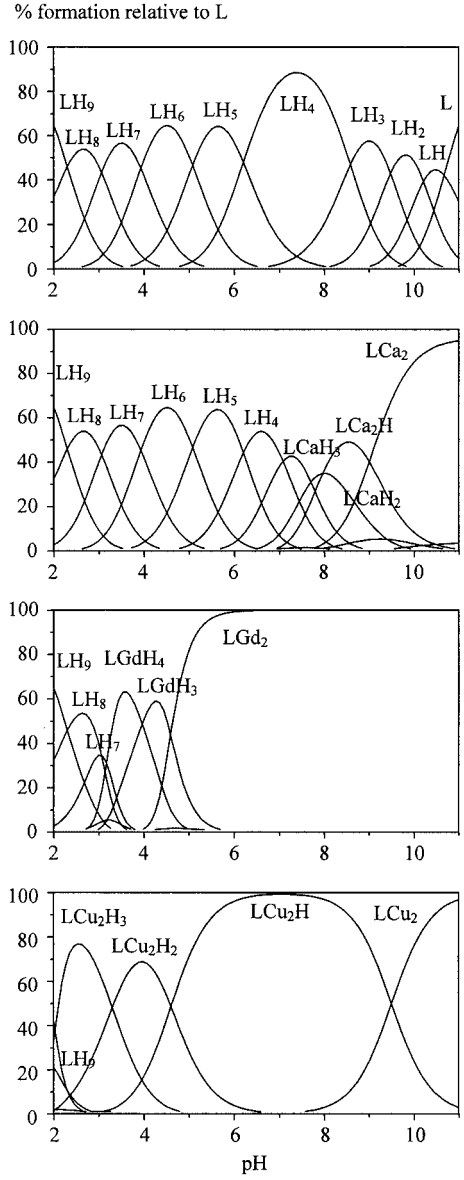

Figure 8. Species distribution diagrams for OHEC and indicated metals (top: calculated for the absence of a coordinating metal). All figures calculated for total concentrations of 5×10^{-4} M ligand and 1×10^{-3} M metal. "L" denotes the deprotonated ligand species OHEC

Comparison of OHEC with Similar Chelators

Macrocyclic OHECs are most easily compared with similar open-chain polyamine polycarboxylic acids by use of the parameter pM, the negative logarithm of the concentration of the free metal species formed at equilibrium for given total concentrations of metal, ligand and pH. Higher pMs indicate stronger complexation since the free metal concentration is depressed to a lower level. This parameter has the advantage that ligands of differing basicity, denticity and nucleacity may be compared directly, which is not the case when the absolute magnitude of stability constants is simply compared. pMs for OHEC and all the studied metals along with the values for the ligands DTPA, DOTA and EDTA are given in Table 7.[21−32] The relatively weak binding properties of OHEC are immediately apparent. Reading across the rows for each metal, OHEC gives rise to the smallest pM amongst all ligands. This is probably due to the binuclear nature of OHEC, such that the second metal centre is always more weakly bound than the first. Nonetheless, the binding strength of OHEC for Gd^{3+} remains very high and similar to that of the commercially applied contrast agents.

Table 7. pM for the ligands OHEC, DTPA, DOTA, and EDTA, calculated for a total metal concentration of 1×10^{-6} M and a total ligand concentration 1×10^{-5} M at pH 7.4; for OHEC the equilibrium constants determined in this work were used, for other ligands literature values were used[22−33]

pM	OHEC	DTPA	DOTA	EDTA
Gd	14.6	18.7	18.9	16.4
Ca	6.0	7.5	11.3	8.4
Cu	15.5	18.1	17.6	17.3
Zn	14.2	15.3	16.0	14.3

Also apparent from Table 7 is the improved selectivity of OHEC for Gd^{3+} over Ca^{2+} with respect to the selectivity of the commercially applied contrast agents DTPA and DOTA. Indeed, the pM for OHEC and Ca^{2+} is 6.0, indicating no complexation of the metal, i.e. all the Ca^{2+} exists as the free cation under the conditions of the calculation. In contrast, OHEC displays a poorer selectivity for Gd^{3+} over the transition metals Cu^{2+} and Zn^{2+}. The pM for OHEC and Zn^{2+} (14.2) approaches that for Gd^{3+} (14.6) while that for Cu^{2+} (15.5) even exceeds that of Gd^{3+}. Thus, the selectivity of OHEC for Gd^{3+} over these latter two transition metals most closely resembles that of EDTA, a ligand whose gadolinium complex gives rise to toxic impacts.[33] However, the in vivo concentration of Ca^{2+} within human blood serum (2.5−4 millimolar)[34] is much higher than the concentrations of Cu^{2+} and Zn^{2+} (1−10 micromolar and 10−50 micromolar, respectively).[34] The high selectivity of OHEC for Gd^{3+} over Ca^{2+} is therefore a positive result for the potential application of this ligand as a contrast agent for MRI.

The relatively weak binding of Ca^{2+} and Gd^{3+} by OHEC is consistent with the presence of propylene bridging groups in this ligand. These give rise to six-membered chelate rings and a significantly reduced "bite-size"[36] (2.5 Å in the idealised conformation) between the chelating nitrogen atoms of the amine. In the corresponding five-membered rings formed by ethylene-bridged amines this bite-size is 2.8 Å for the idealised conformation. The ligands of Table 7 to which OHEC is compared, all contain exclusively ethylene-bridged amines. As has been reviewed,[35] this decrease in bite-size for six-membered chelate rings has virtually no effect on the stability of complexes formed with Cu^{2+} and Zn^{2+} since these metals have relatively small ionic radii, 0.73 and 0.74 Å, respectively.[36] However, for the larger cations Ca^{2+} and Gd^{3+} (ionic radii of 1.12 and 1.053 Å, respectively)[36] the decrease in bite-size reduces complex

stability since the six-membered chelate rings can no longer fully span the metal centres. With Gd^{3+}, however, the complex remains significantly stable since this trivalent cation has a higher charge density than Ca^{2+}. The identical trend in thermodynamic stabilities has been observed for complexes formed between the metals Cu^{2+}, Zn^{2+}, Ca^{2+}, and Gd^{3+} with DOTA and a pair of propylene-bridged derivative ligands.[22,37]

Conclusion

The polyaminocarboxylate macrocycle OHEC ligand developed here can bind two lanthanide ions in close proximity. Homodinuclear lanthanide complexes of OHEC show an interesting coordination equilibrium, depending on the ionic radii of the bound lanthanide ions. Whereas ninefold-coordinated CSAP solid-state structures are found for the mid to early lanthanide(III) ions (Gd, Eu, La) with larger radii, the late lanthanides (Lu, Yb) show eightfold coordination in BCTP structures. These two solid-state structures are the basis for the recently published extensive characterization of the isomerization equilibrium of Ln-OHEC complexes in solution and were used as starting structures for MD calculations.[4]

Ninefold-coordinated Ln-OHEC isomers have one water molecule per lanthanide ion in the inner coordination sphere; this is essential for the efficiency of Gd_2OHEC as a MRI contrast agent. The simultaneous presence of eightfold-coordinated metal centres in solution without water in the first coordination sphere results in a decrease of relaxivity according to the share in the isomerization equilibrium of about 25%.

Nevertheless, OHEC is a useful model ligand in investigating intramolecular electron-spin interactions caused by a short metal−metal distance between paramagnetic lanthanide ions, as shown for the Gd_2OHEC complex. EPR spectra of Gd^{III}- and mixed Gd^{III}/Y^{III} binuclear complexes clearly show that the two Gd^{III} centres interact intramolecularly, resulting in an enhancement of the electronic relaxation of the Gd^{III} electron spins.[38] Other candidates for the investigation of intramolecular electron-spin interactions include bimetallic azacryptates with $Ln^{III}-Ln^{III}$ distances of around 3.5 pm.[39]

The complex solution equilibria of the ligand OHEC have been studied successfully by potentiometry. Using just a single dependent variable, i.e. pH as a function of solution composition, the complete range of solution species and their thermodynamic stabilities could be determined. So much information was extracted from such a simple technique by taking considerable care in the analysis and interpretation of the data. The parameter $\tilde{n}_H$ provided an initial guide in developing a realistic speciation model. Chemical species were included in each metal/ligand/proton system on the basis of their effect upon Σ, the scaled sum of squares. Multiple titrations with suitable variations in concentration and in the metal to ligand ratio were performed for each system. Species that gave rise to highly variable stability constants between independent investigations were viewed as spurious and removed from the model. As a further precaution, titrations were collected for all systems from both forward (vs. KOH) and backward (vs. HCl) titrations. Thus, the equilibrium state was approached from both directions.

The thermodynamic studies revealed that the ligand OHEC is a relatively good chelator for Cu^{2+} and Zn^{2+} while the chelation of Gd^{3+}, and more dramatically Ca^{2+}, is weakened. These trends in complex stability are consistent with the introduction of propylene-bridged amines within the molecular structure of OHEC. The effective deselection of Ca^{2+} by OHEC is a positive result for the potential application of this ligand in a Gd^{3+}-based MRI contrast agent.

Experimental Section

Materials: All reagents used for the preparation of compounds were purchased from either Merck or Aldrich and used as received.

Synthesis: H_8OHEC was prepared by the published method.[1] The sodium salt of the complexes **1** and **2** was prepared by mixing Ln_2O_3, the ligand and NaOH in deionised water (50 mL). The resultant white suspension was heated at 80 °C for several days, until a clear solution was obtained. After cooling to room temperature, the reaction mixture was then filtered and centrifuged to remove undissolved solid material. The final solution was then evaporated to dryness to give a white solid.
Elemental analysis and FAB mass spectra confirmed the composition of the compounds. Elemental analysis: Perkin-Elmer 2400 Series CHNS/O Analyzer. MC: Double-focusing ZAB instrument, VG company (FAB).

X-ray Crystallographic Study: The molecular structures of the complexes **1** and **2** were determined by single-crystal X-ray diffraction. X-ray quality crystals were obtained from saturated aqueous solutions of the pure complexes by slow diffusion of ethanol into the solution of **1** and **2** or by dissolving the solid in a water−ethanol mixture that was kept at 4 °C for several weeks.
Single crystals of compounds **1** and **2** were measured on a STOE Stadi-4 four circle diffractometer at 180 K in a nitrogen atmosphere. Intensity data were corrected for Lorentz, polarisation and absorption (psi-scan technique).[40] Structures were solved by direct methods and refined by full-matrix least-squares against F^2 supported by STOE Xstep software.
Crystal data, data collection and refinement parameters of the structures **1** and **2** are listed in Table 8.
The thermal motion of all non-hydrogen atoms was treated anisotropically, that of hydrogen atoms isotropically and tied 1.2 times higher than the corresponding attached atom.
CCDC-230877 (for **1**) and -230876 (for **2**) contain the supplementary crystallographic data for this paper. These data can be obtained free of charge at www.ccdc.cam.ac.uk/conts/retrieving.html [or from the Cambridge Crystallographic Data Centre, 12 Union Road, Cambridge CB2 1EZ, UK; Fax: (internat.)+44-1223-336-033; E-mail: deposit@ccdc.cam.ac.uk].

NMR Spectroscopy: NMR spectra were recorded on a Bruker AMX 600 and an AVANCE 400 spectrometer equipped with a Silicon Graphics O2 workstation and a HP workstation x1100, respectively. All samples examined were dissolved in deuterated water,

Table 8. Crystal data, details of data collection, and structure refinement for **1** and **2**

Compound	$[Na_2(Yb_2OHEC)]$ (**1**)	$[Na_2(Lu_2OHEC)]$ (**2**)
Crystal data		
Moiety formula	$[C_{34}H_{52}Yb_2N_8O_{16}]^{2-}$, 14,5$H_2O$, C_2H_5OH, 0.5NaOH	$[C_{34}H_{52}Lu_2N_8O_{16}]^{2-}$, 14,5$H_2O$, C_2H_5OH, 0.5NaOH
Space group	$P\bar{1}$ (no. 2)	$P\bar{1}$ (no. 2)
Crystal system	triclinic	triclinic
M_r [amu]	1540.19	1552.06
Crystal size (mm)	0.76 × 0.71 × 0.68	0.78 × 0.51 × 0.38
a [pm]	10.5840(14)	10.569(4)
b [pm]	15.436(2)	15.562(10)
c [pm]	19.1859(17)	19.143(14)
α (°)	110.330(11)	110.48(5)
β (°)	93.837(16)	93.71(5)
γ (°)	106.546(16)	106.67(4)
V [$pm^3 \times 10^6$]	2769.2(6)	2777(3)
$\rho_{calcd.}$ [gcm^{-3}]	1.847	1.856
F (000) [e]	1558	1570
μ(Mo-K_α) [mm^{-1}]	3.477	3.655
Z	2	2
Data collection	Stoe STADI-4	Stoe STADI-4
Radiation λ [pm]	Mo-K_α, 71.073	Mo-K_α, 71.073
T [K]	180	180
Reflections collected	14527	17771
Reflections unique, R_{int}	10298, 0.0328	10904, 0.0228
$2\Theta_{min/max}$ (°)	4.18/50.98	4.18/52.0
h/*k*/*l* ranges	−12,12/ −18,17/ −23,23	−13,13/ −19,18/ −23,23
Refinement	L. S. full-matrix on F^2	L. S. full-matrix on F^2
Data(n)/parameters(p)	10298/798	10904/805
R_1,[a] wR_2[b] [$I > 2\sigma(I)$]	0.0341, 0.0927	0.0264, 0.0642
R_1,wR_2, GoF[c] (all data)	0.0363, 0.0946, 1.109	0.0298, 0.0663, 1.062
$\Delta\rho_{max/min}$ [e $pm^{-3} \times 10^{-6}$]	1.97/−1.95	1.44/−0.91

[a] $R1 = \Sigma(|F_o| - |F_c|)/\Sigma|F_o|$. [b] $wR2 = \{\Sigma[w(F_o^2 - F_c^2)^2]/\Sigma[w(F_o^2)^2]\}^{1/2}$. [c] $GoF = \{[w(F_o^2 - F_c^2)^2]/(n - p)\}^{1/2}$.

which was also used as fixed internal reference. The signal due to residual HDO was suppressed by continuous low-power irradiation. To assign the spectra, 2D and 1D NOE difference experiments were carried out. 2D ^{1}H NMR experiments (H,H-COSY, TOCSY and EXSY) were recorded at 278 K with a sweep-width of δ = 12 ppm for non-paramagnetic compounds and δ = 60 ppm for Eu_2OHEC. Data matrices typically consisted of 4096 complex points in F2 for each of the 1024 F1 increments, the data being zero-filled to a 8192 × 2048 complex matrix before transformation. The EXSY spectrum was recorded using the conventional NOESY phase-sensitive pulse sequence ($90° - t_1 - 90° - \tau_m - 90° -$ acq) with a mixing time of 60 ms.

Solution Thermodynamics: Equilibrium constants were measured at 25 °C in aqueous solution with a supporting electrolyte of 0.1 M KCl. They are defined, Equation (2), as cumulative formation constants (β_{mlh}, where M, L and H refer to the free metal, ligand and proton species, respectively).

$$\beta_{mlh} = \frac{[M_m L_l H_h]}{[M]^m [L]^l [H]^h} \quad (2)$$

Determination of the solution equilibria formed by the ligand OHEC is a challenging problem. The ligand contains 16 donor atoms that simultaneously interact with solution protons and any coordinating metals present. The macrocyclic ring may incorporate up to two metal centres. Ultra-violet/visible spectroscopic measurements were not possible as the ligand is an aliphatic amino-carboxylate. Thus, classical potentiometry was applied.

Apparatus: Titrations were performed in a custom-built 100-mL cell and were held under a positive pressure of N_2 to eliminate ingress of CO_2. The cell was constructed of Pyrex glass with a water jacket for temperature control and a PVC lid with various openings for gas control and insertion of the electrode and burette tips. The glass-bulb pH electrode was obtained from Corning (General Purpose High Performance, catalogue no. 476146). An autoburette from Metrohm (model 716) was employed for titrant delivery and measurement of the electrode potential. The burette was controlled by a personal computer using the LABVIEW[41] programming environment, which allowed automated titration execution. An analytical grade balance (±0.05 mg) was used.

Electrode Calibration: The electrode was calibrated, using a published protocol, over the pH range 2.5 to 11.5 before each titration.[42] Data were analysed using the program GLEE.[43] The parameters E^0 (standard potential), *s* (slope of the electrode) and γ (correction factor of the base concentration) were refined while pK_w was fixed at 13.78.[44,45]

Reagents: All solutions were prepared from deionised (resistivity ≥ 18 MΩ) water. Dissolved CO_2 was removed by boiling and subsequent cooling under N_2. Acid and base solutions (≈0.1 M HCl and KOH) were prepared using Merck Titrisol ampoules and standardized to ±0.2% against potassium hydrogen phthalate (99.95% Aldrich) with phenolphthalein as a visual end-point indi-

cator. Stock solutions of the various metals were prepared in 0.01 M HCl from high purity chloride salts ($GdCl_3$ 99.9% ChemPur, $CaCl_2$ 99% ChemPur, $CuCl_2$ 99.999% Alfa Aesar, $ZnCl_2$ 99.999% Alfa Aesar). These stock solutions were standardised by chelometric titration against a solution of EDTA ($Na_2EDTA{\cdot}2H_2O$ 99% Aldrich) which was in turn standardised by potentiometric titration against an HCl solution. For each metal ion, an appropriate buffer system and indicator dye was used in the chelometric standardisations: for Gd^{3+} Arsenazo III[46] in 0.05 M ammonium acetate, for Ca^{2+} and for Zn^{2+} Xylenol Orange[47] in 6×10^{-4} cetylpyridinium chloride and 0.05 M ammonium acetate adjusted to pH 9, and for Cu^{2+} Xylenol Orange[45] in 0.05 M ammonium acetate adjusted to pH 7. The particular batch of H_8OHEC used for the titrations was isolated as an hydrochloride salt and gave an analytical analysis: $C_{34}H_{60}N_8O_{16}{\cdot}3.5HCl{\cdot}4.5H_2O$ (1044.6): calcd. C 39.1, H 7.0, N 10.7, Cl 11.9; found C 38.7, H 6.5, N 10.4, Cl 12.3.

Titrations: Test solutions were assembled in the titration cell by combining an aliquot of the electrolyte solution (from an A-grade pipette) with a weighed portion of the ligand and, when appropriate, an aliquot of a metal stock solution. Care was taken to add the metal stock solution after dissolution of the ligand to avoid the possibility of metal ion hydrolysis. Concentrations in the range $2.4-9.2\times0^{-4}$ M H_8OHEC were used for protonation studies. Metal complexation experiments employed concentrations of $2.4-9.6\times10^{-4}$ M H_8OHEC and of $0.37-1.7\times10^{-3}$ M for the metal ion, with metal-to-ligand ratios ranging from 1:1 to 1.95:1. In titrations containing the weakly hydrolysed Ca^{2+} an excess of the metal above two equivalents was occasionally used, up to 2.2:1. The resulting solutions typically had an initial pH of ≈3 and were initially titrated to pH 11 with KOH, followed by back titration to pH 2.5 with HCl so that the equilibrium state was approached from both directions. Following addition of titrant the system was allowed to equilibrate for 90 s for ligand-only titrations, 180 s in the presence of a metal, after which time the electrode potential was measured. On obtaining 10 measurements with a standard deviation of ≤0.05 mV the electrode potential was considered stable, a pH measurement was recorded and the titration proceeded to the next point. Each titration contained approximately 120 points, collected between pH 2.5 and 11, each being a measurement of pH versus volume of titrant.

Data Treatment: Equilibrium constants were determined from the titration data by least-squares refinement using the computer program HYPERQUAD.[48] The data from each pair wise set of titrations, i.e. initial titration with KOH and back titration with HCl, were imported into the program along with values for the titrant concentration, initial volume and analytical concentrations of the reagents, as calculated from either the mass of ligand or volume of metal stock taken. The analytical concentration of protons was treated as a refinable parameter, always returning a value within 5% of the initial estimate. The "automatic" weighting scheme was selected with error estimates of 0.002 mL for the titre values and 0.002 pH. Following refinement of the equilibrium constants, the quality of fit was assessed with Σ, the scaled sum of squares, which has an expectation value of one for perfectly fit data. Obtained values ranged between 0.6 and 5.9 with an average of 2.4. Individual species were included into or rejected from the coordination model based on their effect upon Σ. Also, species that gave widely divergent equilibrium constants (standard deviation ≥ 0.5) between independent titrations were rejected. The resulting equilibrium constants, determined from a total of 53 titrations, are given in Table 6.

Acknowledgments

B. O'Sullivan gratefully acknowledges the support of the Alexander von Humboldt Foundation with the awarding of fellowship IV NEU/1070214 STP.

[1] H. Schumann, U. A. Böttger, K. Zietzke, H. Hemling, G. Kociok-Köhn, J. Pickardt, F.-E. Hahn, A. Zschunke, B. Schiefner, H. Gries, B. Radüchel, *Chem. Ber./Recueil* **1997**, *130*, 267−277.
[2] H. Schumann, U. A. Böttger, H. Weisshoff, B. Ziemer, A. Zschunke, *Eur. J. Inorg. Chem.* **1999**, 1735−1743.
[3] H. Schumann, U. A. Böttger, A. Zschunke, H. Weisshoff, B. Ziemer, *Mat. Sc. For.* **1999**, *128*, 315−317.
[4] G. M. Nicolle, Y. Fabrice, D. Imbert, U. A. Böttger, J.-C. Bünzli, A. E. Merbach, *Chem. Eur. J.* **2003**, *9*, 5453−5467.
[5] J. Dale, *Isr. J. Chem.* **1980**, *20*, 3−11.
[6] C. W. Haigh, *Polyhedron* **1995**, *14*, 2871−2878.
[7] E. L. Muetterties, L. J. Guggenberger, *J. Am. Chem. Soc.* **1974**, *96*, 1748−1756.
[8] S. Aime, A. Barge, M. Botta, M. Fasano, J. D. Ayala, G. Bombieri, *Inorg. Chim. Acta* **1996**, *26*, 423−429.
[9] F. Benetello, G. Bombieri, L. Calabi, S. Aime, M. Botta, *Inorg. Chem.* **2003**, *42*, 148−157.
[10] K. Micskei, L. Helm, E. Brücher, A. E. Merbach, *Inorg. Chem.* **1993**, *32*, 3844−3850.
[11] M.-R. Spirlet, J. Rebizant, J. F. Desreux, M.-F. Loncin, *Inorg. Chem.* **1984**, *23*, 359−363.
[12] J. A. Peters, E. Zitha-Bovens, D. M. Corsi, C. F. G. C. Geraldes, *The Chemistry of Contrast Agents in Medical Magnetic Resonance Imaging*, **2001**, p. 315−382.
[13] F. Uggeri, S. Aime, P. L. Anelli, M. Botta, M. Brochetta, C. DeHaen, G. Ermondi, M. Grandi, *Inorg. Chem.* **1995**, *34*, 633−642.
[14] S. Aime, M. Botta, M. Fasano, M. P. M. Marques, C. F. G. C. Geraldes, D. Pubanz, A. E. Merbach, *Inorg. Chem.* **1997**, *36*, 2059−2068.
[15] E. Bovens, M. A. Hoefnagel, E. Boers, H. Lammers, H. van Bekkum, J. A. Peters, *Inorg. Chem.* **1996**, *35*, 7679−7683.
[16] S. Aime, A. Barge, A. Borel, M. Botta, S. Chemerisov, A. E. Merbach, U. Müller, D. Pubanz, *Inorg. Chem.* **1997**, *36*, 5104−5112.
[17] É. Tóth, *The Chemistry of Contrast Agents in Medical Magnetic Resonance Imaging*, **2001**, p. 74−78.
[18] H. D. Powell, O. M. Ni Dhubhghaill, D. Pubanz, L. Helm, Y. Lebedev, W. Schlaepfer, A. E. Merbach, *J. Am. Chem. Soc.* **1996**, *118*, 9333−9346.
[19] E. Tóth, D. Pubanz, S. Vauthey, L. Helm, A. E. Merbach, *Chem. Eur. J.* **1996**, *2*, 1607−1615.
[20] E. Tóth, F. Connac, L. Helm, K. Adzamli, A. E. Merbach, *Eur. J. Inorg. Chem.* **1998**, 2017−2021.
[21] E. T. Clarke, A. E. Martell, *Inorg. Chim. Acta* **1991**, *190*, 27−36.
[22] E. W. Baumann, *J. Inorg. Nucl. Chem.* **1974**, *16*, 1827−1832.
[23] G. Anderegg, P. Nägeli, F. Müller, G. Schwarzenbach, *Helv. Chim. Acta* **1959**, *42*, 827−836.
[24] A. P. Brunetti, G. H. Nancollas, P. N. Smith, *J. Am. Chem. Soc.* **1969**, *91*, 4680−4683.
[25] J. D. Carr, D. G. Swartzfager, *J. Am. Chem. Soc.* **1975**, *97*, 315−321.
[26] S. Chaberek, A. E. Frost, M. A. Doran, N. J. Bicknell, *J. Inorg. Nucl. Chem.* **1959**, *11*, 184−196.
[27] R. Delgado, J. J. R. Fraústo Da Silva, *Talanta* **1982**, *29*, 815−822.
[28] E. J. Durham, D. P. Ryskiewich, *J. Am. Chem. Soc.* **1958**, *80*, 4812−4817.
[29] C. Gèze, C. Mouro, F. Hindré, M. Le Plouzennec, C. Moinet, R. Rolland, L. Alderighi, A. Vacca, G. Simmoneaux, *Bull. Soc. Chim. France* **1996**, *133*, 267−272.
[30] T. F. Gritmon, M. P. Goedken, G. R. Choppin, *J. Inorg. Nucl. Chem.* **1977**, *39*, 2021−2023.

[31] K. Kumar, C. Allen Chang, L. C. Francesconi, D. D. Dischino, M. F. Malley, J. Z. Gougoutas, M. F. Tweedle, *Inorg. Chem.* **1994**, *33*, 3567−3575.
[32] R. A. Overvoll, W. Lund, *Anal. Chim. Acta* **1982**, *143*, 153−161.
[33] R. B. Lauffer, *Chem. Rev.* **1987**, *87*, 901−927.
[34] W. P. Cacheris, S. C. Quay, S. M. Rocklage, *Mag. Res. Imag.* **1990**, *8*, 467−481.
[35] R. D. Hancock, *J. Chem. Educ.* **1992**, *69*, 615−621.
[36] R. D. Shannon, *Acta Crystallogr., Sect. A* **1976**, *32*, 751−767.
[37] E. T. Clarke, A. E. Martell, *Inorg. Chim. Acta* **1991**, *190*, 37−46.
[38] G. M. Nicolle, L. Helm, A. E. Merbach, *Magn. Res. Chem.* **2003**, *41*, 794−799.
[39] F. Avecilla, C. Platas-Iglesias, R. Rodríguez-Cortiñas, G. Guillemot, J.-C. G. Bünzli, C. D. Brondino, C. F. G. C. Geraldes, A. de Blas, T. Rodríguez-Blas, *J. Chem. Soc., Dalton Trans.* **2002**, 4658−4665.
[40] N. Walker, D. Stuart, *Acta Crystallogr., Sect. A* **1983**, *39*, 158−166.
[41] *LABVIEW, 6.1*, National Instruments Corporation, http://www.ni.com/, 11500 N Mopac Expwy, Austin, TX 78759−3504.
[42] A. R. Johnson, B. O′Sullivan, K. N. Raymond, *Inorg. Chem.* **2000**, *39*, 2652−2660.
[43] P. Gans, B. O′Sullivan, *Talanta* **2000**, *51*, 33−37.
[44] H. S. Harned, B. B. Owen, *The Physical Chemistry of Electrolytic Solutions*, Reinhold Pub. Corp., New York, **1958**, p. 803.
[45] F. H. Sweeton, R. E. Mesmer, C. F. J. Baes, *J. Sol. Chem.* **1974**, *3*, 191−196.
[46] K. Ueno, T. Imamura, K. L. Cheng, *Handbook of Organic Analytical Reagents*, CRC Press, Boca Raton, FL, **1992**, p. 615.
[47] V. Svoboda, V. Chromý, *Talanta* **1965**, *12*, 431−436.
[48] P. Gans, A. Sabatini, A. Vacca, *Talanta* **1996**, *43*, 1739−1753.

Received February 15, 2004
Early View Article
Published Online August 12, 2004

